Connecting heterogeneous quantum networks by hybrid entanglement swapping

Giovanni Guccione, Tom Darras, Hanna Le Jeannic, Varun B Verma, Sae Woo Nam, Adrien Cavaillès, Julien Laurat

PHYSICS

Connecting heterogeneous quantum networks by hybrid entanglement swapping

Giovanni Guccione[1]*, Tom Darras[1]*, Hanna Le Jeannic[1†], Varun B. Verma[2], Sae Woo Nam[2], Adrien Cavaillès[1‡], Julien Laurat[1‡]

Recent advances in quantum technologies are rapidly stimulating the building of quantum networks. With the parallel development of multiple physical platforms and different types of encodings, a challenge for present and future networks is to uphold a heterogeneous structure for full functionality and therefore support modular systems that are not necessarily compatible with one another. Central to this endeavor is the capability to distribute and interconnect optical entangled states relying on different discrete and continuous quantum variables. Here, we report an entanglement swapping protocol connecting such entangled states. We generate single-photon entanglement and hybrid entanglement between particle- and wave-like optical qubits and then demonstrate the heralded creation of hybrid entanglement at a distance by using a specific Bell-state measurement. This ability opens up the prospect of connecting heterogeneous nodes of a network, with the promise of increased integration and novel functionalities.

INTRODUCTION

When looking at compatibility issues in quantum information processing and networks, light is an emblematic example. Its use has historically been split between two communities depending on the degree of freedom favored for encoding. On one side is the continuous-variable (CV) approach, which treats optical fields as waves (*1*). On the other side is the discrete-variable (DV) approach, harnessing the properties of individual photons (*2*). These two strategies have been studied extensively and led to a variety of seminal demonstrations for quantum technologies with complementary advantages (*3*, *4*). By considering a hybrid approach bridging the two, one could envision a quantum network where the two encodings can be interchanged fittingly to the task at hand. This conversion could also find applications for connecting disparate quantum devices (*5*), e.g., CV oscillators and finite-level DV systems, which can couple preferentially to one or the other optical degree of freedom. Achieving this versatility is a critical challenge for developing a modular approach to quantum networks.

Several experiments have spearheaded the development of the hybrid quantum optics paradigm (*6*–*8*). The first realizations from a decade ago consisted in combining the DV and CV toolboxes to generate non-Gaussian states, such as optical Schrödinger cat states starting from Gaussian squeezed light (*9*–*11*). These advances spurred intense experimental and theoretical efforts toward novel protocols, including deterministic teleportation of photonic qubits (*12*) or witnesses for single-photon entanglement based on CV homodyne measurements (*13*). More recently, the engineering of hybrid entanglement of light (*14*–*16*), i.e., entanglement between particle- and wave-like optical qubits, enabled remote state preparation (*17*) and teleportation between different encodings (*18*, *19*). This entanglement was also certified for use in one-sided device-independent protocols (*20*).

In this context, a hybrid network requires an original approach to link and transfer entanglement between diverse nodes (*21*). A cornerstone capability is thereby given by entanglement swapping, which is at the foundation of quantum repeaters (*22*, *23*). Entanglement swapping was originally performed for DV systems (*24*) before being extended to CV schemes (*25*, *26*). A swapping technique

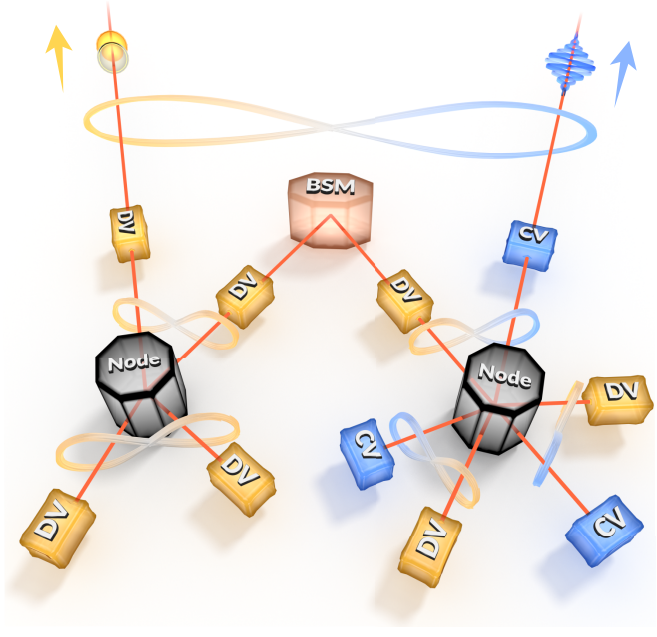

Fig. 1. A heterogeneous quantum network linked by entanglement swapping. A DV node, on the left, establishes a link to a hybrid node, on the right, via a swapping protocol implemented by a Bell-state measurement (BSM) at an intermediate station. Hybrid CV-DV entanglement is created between two modes that never interacted. The resulting entangled state is available to perform subsequent remote state preparation, to enable teleportation-based encoding conversion, or to connect disparate physical platforms at longer distances.

[1]Laboratoire Kastler Brossel, Sorbonne Université, CNRS, ENS-Universite PSL, Collège de France, 4 Place Jussieu, 75005 Paris, France. [2]National Institute of Standards and Technology, 325 Broadway, Boulder, CO 80305, USA.
*These authors contributed equally to the work.
†Present address: Center for Hybrid Quantum Networks (Hy-Q), Niels Bohr Institute, University of Copenhagen, Blegdamsvej 17, DK-2100 Copenhagen, Denmark.
‡Corresponding author. Email: adrien.cavailles@lip6.fr (A.C.); julien.laurat@sorbonne-universite.fr (J.L.)

combining the salient characteristic from the two optical paradigms has also been recently demonstrated to transfer DV entanglement via CV entanglement (*27*). However, the distribution of hybrid CV-DV entanglement of light by entanglement swapping has not been addressed until now.

In this work, we report an entanglement swapping protocol where two end nodes arrive at sharing hybrid CV-DV entanglement despite one of the initial stations starting as a DV-only platform. The scenario is sketched in Fig. 1, where a DV node establishes a quantum link with a hybrid CV-DV node after swapping is heralded by a specific Bell-state measurement (BSM) at a central station. Specifically, in our experiment, we created single-photon entanglement and hybrid entanglement and then performed swapping using a measurement involving a single-photon counter and a homodyne detection. Entanglement between the modes that never interacted was lastly verified by full quantum state tomography. Our experiment thereby provides a crucial capability of communication in heterogeneous networks. This entanglement distribution has also been shown to be advantageous for optics-based quantum computation (*28*), loss-resilient quantum key distribution (*29*), and entanglement purification (*30*, *29*).

RESULTS

Experimental setup and initial entangled states

The experimental scheme is presented in Fig. 2. Our implementation is an adaptation of the scenario in Fig. 1 where the two input entangled states are generated in sequence using the same resources. More specifically, the CV and DV components of the initial entangled states are respectively derived from single- and two-mode squeezed vacua generated by parametric down conversion from two optical parametric oscillators (OPO I for single-mode and OPO II for two-mode). The OPOs are driven well below threshold to ensure high fidelity with the expected states (see Materials and Methods). The two-mode squeezer is used at two consecutive times to generate first the single-photon entanglement and then the DV component of the hybrid entangled state. Overall, the experiment amounts to the use of five independent single-mode squeezers. This time-multiplexed usage of the quantum state sources is, however, specific to our implementation and not intrinsic to the swapping protocol hereby presented. The addition of a fast switch would enable the full spatial separation of the modes (see the Supplementary Materials).

Specifically, our realization starts with the generation of single-photon entanglement. A polarizing beamsplitter placed at the output of OPO II separates the signal and idler modes. The idler mode is channeled to a heralding station, where it can be detected after filtering by a high-efficiency superconducting nanowire single-photon detector (SNSPD) (*31*), with a system detection efficiency of about 85% and dark noise below 10 counts/s. A first detection event on SNSPD α heralds the presence of a single photon in the signal mode. The photon propagates to a 50:50 plate where it is split between modes A and B, generating the DV entangled state, up to a normalization factor

$$|\Phi\rangle_{AB} \propto |0\rangle_A|1\rangle_B + |1\rangle_A|0\rangle_B \quad (1)$$

Mode B is then directed to a 47-ns delay line in free space (see the Supplementary Materials).

Next, hybrid CV-DV entanglement is created. For this purpose, a small fraction of the single-mode squeezed vacuum (3%) is tapped

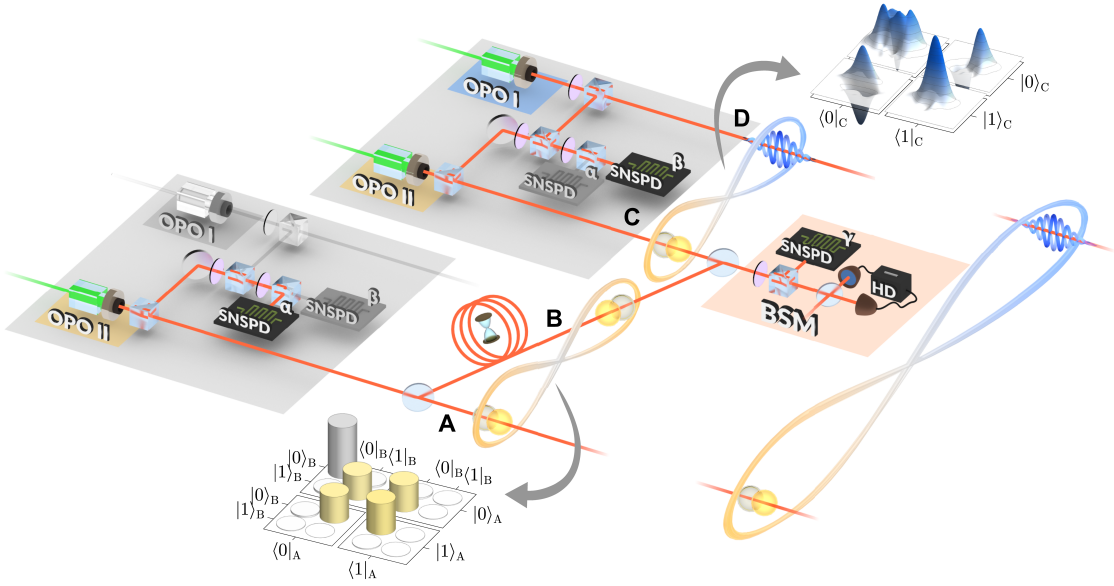

Fig. 2. Experimental setup. The gray panels outline the nonlinear sources and operations, i.e., optical parametric oscillators and heralding measurements. CV states are produced via a single-mode squeezer (OPO I), while DV states are generated by a two-mode squeezer (OPO II). The sources are used at different times to generate DV single-photon entanglement between modes A and B first and hybrid DV-CV entanglement between modes C and D afterward. The matrices show the measured entangled states: single-photon entanglement heralded by superconducting nanowire single-photon detector (SNSPD) α (bottom) and hybrid entanglement heralded by SNSPD β (top, Wigner representation of the reduced states). To prepare for entanglement swapping, a delay line holds off the state in mode B to enable the temporal matching of one DV mode from each of the two initial states. These modes are mixed at the BSM station (light brown panel), where a combination of a detection event on SNSPD γ and a quadrature measurement via homodyne detection (HD) is performed. Upon success, hybrid entanglement is heralded between modes A and D where high-efficiency homodyne detections are used for full two-mode quantum state tomography.

off and mixed with the idler mode of OPO II. A detection event, now on SNSPD β, heralds the entangled state (*14*).

$$|\Psi\rangle_{CD} \propto |0\rangle_C |\mathrm{cat}_-\rangle_D + |1\rangle_C |\mathrm{cat}_+\rangle_D \quad (2)$$

Here, $|\mathrm{cat}_+\rangle$ and $|\mathrm{cat}_-\rangle$ denote, respectively, the even and odd optical Schrödinger cat states (*8*) forming the basis of our CV qubit space, corresponding to superpositions of coherent states of amplitude $a \approx 0.9$. The single-mode squeezed vacuum and the photon-subtracted squeezed vacuum states generated by the OPO can concurrently reach fidelities above 90% with these states at moderate squeezing levels of about 5 dB. Details on this measurement-induced preparation have been reported elsewhere (*14*).

Realization of entanglement swapping

Given the successful generation of both initial entangled states, with the adequate delay between heralding events (see the Supplementary Materials), typically at a rate of 140 events/s, entanglement swapping is then performed. The output of the delay line, mode B, and the DV component of the hybrid state, mode C, are brought to interfere on a 50:50 beamsplitter, leading to the combined state

$$\begin{aligned} |\psi_{BSM}\rangle \propto \sqrt{2}\,|0\rangle_B|0\rangle_C \otimes |1\rangle_A|\mathrm{cat}_-\rangle_D \\ +|0\rangle_B|1\rangle_C \otimes (|0\rangle_A|\mathrm{cat}_-\rangle_D + |1\rangle_A|\mathrm{cat}_+\rangle_D) \\ +|1\rangle_B|0\rangle_C \otimes (|0\rangle_A|\mathrm{cat}_-\rangle_D - |1\rangle_A|\mathrm{cat}_+\rangle_D) \\ +(|0\rangle_B|2\rangle_C - |2\rangle_B|0\rangle_C) \otimes |0\rangle_A|\mathrm{cat}_+\rangle_D \end{aligned} \quad (3)$$

If one (and exactly one) photon is detected on either of the outputs, then modes A and D become hybrid entangled without ever directly interacting. We consider only detection events on mode C to ensure that we always recover the same state $|\Psi\rangle_{AD}$ at the output. We also note that at every stage of our experiment, active phase stabilization of the different paths is a critical requirement (see Materials and Methods).

To realize the single-photon projection, the BSM consists of two parts: a low-reflectivity beamsplitter (R = 10%) to tap off a small fraction of light, which is sent to a single-photon detector (SNSPD γ), and a homodyne setup for quadrature measurement. The role of the SNSPD is to herald a photon subtraction from mode C. The homodyne measurement is then used to condition on the quadrature of the state after subtraction to conclude the projection and thereby trigger a successful BSM (see Materials and Methods). More details on key parameters are provided in the Supplementary Materials. In our specific case, because of the use of a delay line, the beamsplitter for the BSM corresponds to the one used to create the single-photon entangled state, this time accessed from the other input port. This beamsplitter would be distinct in a general scenario involving two separate sources. Overall, the whole procedure inclusive of state preparation and filtering for successful swapping—i.e., three single-photon detections and one homodyne conditioning—occurs at a rate of about three events/min.

Characterization of the entangled states

We now turn to the experimental results. The quantum states involved in our experiment are shown in Fig. 3. They are measured by quantum state tomography performed with two high-efficiency homodyne detections and reconstructed via maximum-likelihood algorithms (*32*).

We first show, on the left-hand side, the two initial heterogeneous entangled inputs: single-photon DV-DV entanglement (top) and hybrid CV-DV entanglement (bottom). To characterize the DV-DV input, we used homodyne tomography on mode A directly and on mode B after the delay line. The DV-DV state shown in Fig. 3 is corrected only for homodyne detection loss, corresponding to 18% for both modes. Similarly, the hybrid CV-DV input has been reconstructed using homodyne tomography on modes C (without the delay line's beamsplitter) and D. In this case, the detection loss amounts to 17% for the DV mode and 15% for the CV mode. For the two initial states, with these measurements in hand, we lastly computed the negativity of entanglement (*33*) given by $\mathcal{N} = (\|\rho^{T_X}\|_1 - 1)/2$,

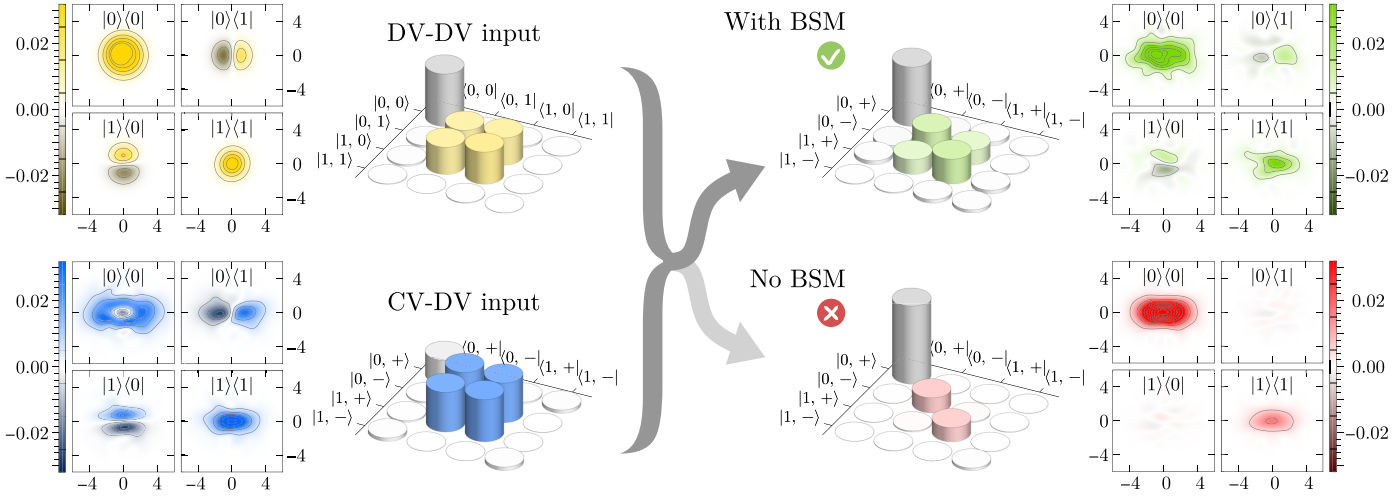

Fig. 3. Entanglement swapping results. Tomographic measurements of the initial entangled states are given on the left, with DV-DV entanglement at the top and hybrid CV-DV entanglement at the bottom. The right side provides the measurement of the output state when the BSM heralds entanglement swapping and, for reference, when no BSM is implemented (see the Supplementary Materials for more specific comparison). All states are displayed using two representations, a hybrid density-Wigner plot and a density matrix giving the reconstructed state projected in the relevant basis (vacuum–single-photon $\{|0\rangle, |1\rangle\}$ for DV and coherent-state superpositions $\{|\mathrm{cat}_+\rangle, |\mathrm{cat}_-\rangle\}$ for CV). The number of tomographic samples for each state reconstruction is 600,000; 200,000; 7800; and 200,000 respectively. For simplicity, only the real part of the density matrices is shown, as the imaginary part consists of near-zero elements of magnitude smaller than 1%. The input states coincide with those featured in Fig. 2.

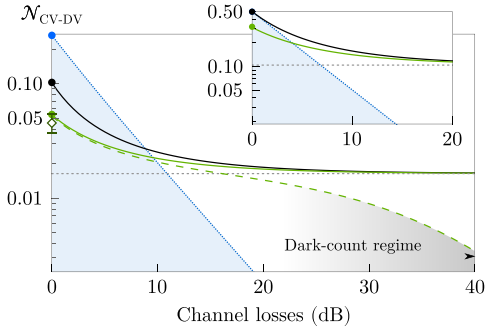

Fig. 4. Swapping for remote hybrid entanglement distribution. The expected entanglement negativity after swapping of the experimental initial resources is evaluated as a function of the channel loss (considered symmetric on the two channels). The black solid line corresponds to an ideal BSM with vanishing reflectivity R and quadrature conditioning window Δ, while the green line corresponds to the implemented case ($R = 10\%$ and Δ equal to the vacuum shot noise). The gray dotted line corresponds to a BSM without homodyne conditioning. The effect of dark counts is presented by the green dashed line (1% of total events). The white point gives the measured output negativity, in good agreement with the simulation. As a reference, the blue line shows the negativity for direct propagation. The inset provides the same plots but starting from maximally entangled input states and without dark counts.

where ρ^{T_X} stands for the partial transpose of the two-mode density matrix ρ_{XY} with respect to mode X. This quantity reaches 0.5 for an ideal maximally entangled state. We obtained 0.099 ± 0.002 for single-photon entanglement and 0.223 ± 0.003 for hybrid entanglement. These values are set by the initial purity of the generated states, slightly degraded relative to previous works from our group (*14*, *31*) due to a larger pumping power that was necessary to increase the operating rates and also owing to the optical losses in the complex circuit that involves the delay loop.

Next, on the right-hand side of Fig. 3, we provide the output state between modes A and D. As the homodyne setup used for tomography of the DV mode is also the one used for the BSM, an additional 10% loss due to the low-reflectivity beamsplitter used for photon subtraction is added. A total loss of 26% on the DV mode and 15% on the CV mode is corrected for the reconstruction. The output state at the top corresponds to the outcome when the BSM is successfully implemented. Given this swapping heralding event, nonzero off-diagonal coherence terms appear, thereby confirming the emergence of quantum correlations, although the modes have never directly interacted. We further assessed the success of the swapping protocol by computing the negativity of entanglement, estimated at 0.044 ± 0.009 (see the Supplementary Materials). Last, we repeated the experiment under the same conditions but without the BSM. As shown by the state at the bottom, the output modes are not correlated, and no entanglement can be observed in this case. These results show the ability to swap between disparate optical entangled states and to establish hybrid CV-DV entanglement between heterogeneous nodes.

DISCUSSION

The swapping process is of paramount importance in the context of quantum connection as it allows the distribution of entanglement over nodes that would be too distant for direct propagation. Thus, in Fig. 4, we provide theoretical predictions of the negativity of entanglement as a function of transmission losses. In particular, starting from our initial experimental states or from maximally entangled states (inset), we compute the negativity of entanglement of the output hybrid state under different BSM implementations and compare to direct propagation in the most resilient case of symmetric losses on the two transmission channels. The white point indicates our measurement, in good agreement with the simulations.

As can be seen, the swapping protocol would beat the direct propagation for losses over 4 dB (about 20 km of fiber at telecom wavelength) for maximally entangled input states and over 9 dB (about 45 km) under our experimental conditions. We also note that homodyne conditioning leads to an increase in entanglement compared to a partial BSM (i.e., performed with only single-photon detection and no homodyne conditioning). This is most notable over shorter distances and in the case of highly entangled input states where the two-photon component after mixing is larger. Ultimately, any practical implementation of the protocol will be limited by the heralding rate of the input states and its ratio with the dark-count rate of the used detectors. In our experiment, where the ratio is approximately 1:100, we expect a substantial decrease of negativity over 20 dB of channel losses, as shown in Fig. 4. Additional consequences linked to the state reconstruction and false-positive events are detailed in the Supplementary Materials. These results confirm the protocol's performance and that its demonstration over long distances could be achieved in future implementations, although with increasingly challenging rates.

For practical operations, the protocol's success rates will need to be greatly improved. The current limits are primarily due to the probabilistic nature of the generation process. Different paths are being developed to solve this general bottleneck in quantum technology when cascaded operations are performed. Better synchronization of heralded probabilistic resources, as implemented in recent works with high state purity (*34*, *35*), or extension of quantum state engineering and of the hybrid approach to on-demand non-Gaussian sources (*36*, *37*) are promising directions. Implementations at telecom wavelength, or with dual frequencies, would also be possible given the current developments of efficient squeezers in this regime (*38*).

In conclusion, our work introduced and demonstrated an entanglement swapping protocol that connects nodes with different optical encodings. This core capability opens attractive opportunities for the establishment of remote hybrid quantum links and the development of heterogeneous quantum networks, enabling more versatile quantum information interconnects. An exciting future prospect will be to couple such hybrid entanglement to matter systems and to link thereby not only different encodings but also quantum devices of a different nature with complementary functionalities.

MATERIALS AND METHODS

Quantum state engineering

The triply resonant OPOs are based on broadband (65 MHz) semimonolithic linear cavities, pumped below threshold by a frequency-doubled Nd:YAG laser (InnoLight GmbH). For both cavities, the input mirror is directly coated on one face of the nonlinear crystal, with high reflectivity at 1064 nm and 95% reflectivity at the 532 nm pump wavelength. The output mirrors have a radius of curvature of 38 mm and a coating with 90% reflectivity at 1064 nm and high reflectivity at 532 nm. For this experiment, OPO I (10-mm type-I phase-matched PPKTP Raicol Crystals) was pumped by 15 mW of 532-nm light (80% below threshold, squeezing of about 5 dB), while

OPO II (10-mm type-II KTP Raicol Crystals) was pumped by 5 mW (95% below threshold to limit the multiphoton components). The hybrid entangled state is produced by combining the tapped beam from OPO I and the idler beam from OPO II and projecting them onto the same mode with a polarizing beamsplitter. The state, heralded on SNSPD β, is maximally entangled when the polarizations before the beamsplitter are rotated to have equal counts from each OPO (*16*). This balancing condition places a constrain on the relative counts on the other port of the beamsplitter. With N_I (N_{II}) being the count rates from OPO I (II), a detector on the unbalanced port would see events at a rate of $|N_{II}^2 - N_I^2|/(N_I^2 + N_{II}^2)$. In our case, this corresponds to 92% of photons coming from OPO II. This strong imbalance enables the heralding of a single photon used for DV entanglement on SNSPD α. Before detection on the SNSPDs, the nondegenerate modes of the OPOs are filtered out using a 0.5-nm bandwidth interferential filter (Barr Associates) and a home-made Fabry-Pérot cavity (free spectral range, 330 GHz; bandwidth, 320 MHz).

Experimental lockings and phase stability

The two OPO cavities are locked on resonance using the Pound-Drever-Hall technique (12-MHz phase modulation on the pump). Seed beams at 1064 nm, originating from a triangular tilt-locked mode-cleaner cavity (length, 40 cm), are used for phase calibrations. They are first phase-locked with each pump using microcontrollers (ADuC7020 Analog Devices, 1% phase noise). The relative phase between the conditioning paths from the OPOs I and II, as well as the filtering cavities, are digitally locked (3% phase noise) using the same technique. The free-space delay line is digitally locked (Newport LB1005 Servo Controller) on a Fano-like resonance shape obtained by slightly tilting the polarization of the beam before self-interference, in a technique similar to the Hänsch-Couillaud scheme (3% phase noise). The seed beams are also used for phase calibration of the homodyne detections. Apart from the mode cleaner and OPO cavities, all locks are performed under a sampling-and-hold cycle: with the SNSPDs shut off, the locks are readjusted during a 50-ms time window, thanks to the 1064-nm seed beams; then, the SNSPDs paths are reactivated to acquire the data during the following 50 ms while the seed beams are off.

The Bell-state measurement

The BSM consists of the following two operations: photon subtraction and quadrature conditioning. The subtraction is implemented by a low-reflectivity beamsplitter. The probability of subtracting a single photon scales linearly with the reflectivity, whereas the probability of a two-photon subtraction scales quadratically. It is thus important to operate in the limit of small reflectivity. Once a single-photon subtraction is heralded, the $|1\rangle_C$ element in the state $|\psi_{BSM}\rangle$ (Eq. 3) reduces to a vacuum state, $|0\rangle_C$. The homodyne measurement is used to favor this vacuum term over other unwanted contributions, i.e., the former two-photon term reduced to a single-photon contribution after subtraction. Having different marginal distributions, the two states have different probability of returning a given quadrature value, meaning that they can be discriminated if the outcome is conditioned to be around a specific point where the states would be orthogonal. Specifically, the probability of detecting a vanishing quadrature value is high for vacuum and negligible for a single photon. In our experiment, we use a beamsplitter reflection of 10% and a homodyne conditioning window spanning half the standard deviation of the vacuum shot noise on either side of the origin (with a probability overlap of 8% between the two states to be discriminated). The requirements for both of these parameters can be relaxed or strengthened to trade between fidelity and success rate (see the Supplementary Materials). Note that in our case, where the two-photon component is negligible, the efficiency of the SNSPD does not affect the fidelity of the swapped state but only the success rate. On the contrary, the efficiency of the homodyne detection is crucial for the fidelity. This problem is mitigated by the availability of photodiodes with near-unity efficiency.

SUPPLEMENTARY MATERIALS

Supplementary material for this article is available at http://advances.sciencemag.org/cgi/content/full/6/22/eaba4508/DC1

REFERENCES AND NOTES

1. S. L. Braunstein, P. van Loock, Quantum information with continuous variables. *Rev. Mod. Phys.* **77**, 513–577 (2005).
2. P. Kok, Linear optical quantum computing with photonic qubits. *Rev. Mod. Phys.* **79**, 135–174 (2007).
3. J. L. O'Brien, A. Furusawa, J. Vucković, Photonic quantum technologies. *Nat. Photonics* **3**, 687–695 (2009).
4. I. A. Walmsley, Quantum optics: Science and technology in a new light. *Science* **348**, 525–530 (2015).
5. G. Kurizki, P. Bertet, Y. Kubo, K. Mølmer, D. Petrosyan, P. Rabl, J. Schmiedmayer, Quantum technologies with hybrid systems. *Proc. Natl. Acad. Sci. U.S.A.* **112**, 3866–3873 (2015).
6. P. van Loock, Optical hybrid approaches to quantum information. *Laser Photonics Rev.* **5**, 167–200 (2011).
7. U. L. Andersen, J. S. Neergaard-Nielsen, P. van Loock, A. Furusawa, Hybrid discrete- and continuous-variable quantum information. *Nat. Phys.* **11**, 713–719 (2015).
8. P. Minzioni, C. Lacava, T. Tanabe, J. Dong, X. Hu, G. Csaba, W. Porod, G. Singh, A. E. Willner, A. Almaiman, Roadmap on all-optical processing. *J. Opt.* **21**, 063001 (2019).
9. M. Dakna, T. Anhut, T. Opatrný, L. Knöll, D.-G. Welsch, Generating Schrödinger-cat-like states by means of conditional measurements on a beam splitter. *Phys. Rev. A* **55**, 3184–3194 (1997).
10. A. Ourjoumtsev, R. Tualle-Brouri, J. Laurat, P. Grangier, Generating optical Schrödinger kittens for quantum information processing. *Science* **312**, 83–86 (2006).
11. J. S. Neergard-Nielsen, B. M. Nielsen, C. Hettich, K. Molmer, E. S. Polzik, Generation of a superposition of odd photon number states for quantum information networks. *Phys. Rev. Lett.* **97**, 083604 (2006).
12. S. Takeda, T. Mizuta, M. Fuwa, P. van Loock, A. Furusawa, Deterministic quantum teleportation of photonic quantum bits by a hybrid technique. *Nature* **500**, 315–318 (2013).
13. O. Morin, J.-D. Bancal, M. Ho, P. Sekatski, V. D'Auria, N. Gisin, J. Laurat, N. Sangouard, Witnessing trustworthy single-photon entanglement with local homodyne measurements. *Phys. Rev. Lett.* **110**, 130401 (2013).
14. O. Morin, K. Huang, J. Liu, H. L. Jeannic, C. Fabre, J. Laurat, Remote creation of hybrid entanglement between particle-like and wave-like optical qubits. *Nat. Photonics* **8**, 570–574 (2014).
15. H. Jeong, A. Zavatta, M. Kang, S.-W. Lee, L. S. Costanzo, S. Grandi, T. C. Ralph, M. Bellini, Generation of hybrid entanglement of light. *Nat. Photonics* **8**, 564–569 (2014).
16. K. Huang, H. Le Jeannic, O. Morin, T. Darras, G. Guccione, A. Cavaillès, J. Laurat, Engineering optical hybrid entanglement between discrete- and continuous-variable states. *New J. Phys.* **21**, 083033 (2019).
17. H. Le Jeannic, A. Cavaillès, J. Raskop, K. Huang, J. Laurat, Remote preparation of arbitrary continuous-variable qubits using loss-tolerant hybrid entanglement of light. *Optica* **5**, 1012–1015 (2018).
18. A. E. Ulanov, D. Sychev, A. A. Pushkina, I. A. Fedorov, A. I. Lvovsky, Quantum teleportation between discrete and continuous encodings of an optical qubit. *Phys. Rev. Lett.* **118**, 160501 (2017).
19. D. V. Sychev, A. E. Ulanov, E. S. Tiunov, A. A. Pushkina, A. Kuzhamuratov, V. Novikov, A. I. Lvovsky, Entanglement and teleportation between polarization and wave-like encodings of an optical qubit. *Nat. Commun.* **9**, 3672 (2018).
20. A. Cavaillès, H. Le Jeannic, J. Raskop, G. Guccione, D. Markham, E. Diamanti, M. D. Shaw, V. B. Verma, S. W. Nam, J. Laurat, Demonstration of einstein-podolsky-rosen steering using hybrid continuous- and discrete-variable entanglement of light. *Phys. Rev. Lett.* **121**, 170403 (2018).
21. S. Wehner, D. Elkouss, R. Hanson, Quantum internet: A vision for the road ahead. *Science* **362**, eaam9288 (2018).

22. H.-J. Briegel, W. Dür, J. I. Cirac, P. Zoller, Quantum repeaters: The role of imperfect local operations in quantum communication. *Phys. Rev. Lett.* **81**, 5932–5935 (1998).
23. L.-M. Duan, M. D. Lukin, J. I. Cirac, P. Zoller, Long-distance quantum communication with atomic ensembles and linear optics. *Nature* **414**, 413–418 (2001).
24. J. W. Pan, D. Bouwmeester, H. Weinfurter, A. Zeilinger, Experimental entanglement swapping: Entangling photons that never interacted. *Phys. Rev. Lett.* **80**, 3891–3894 (1998).
25. X. Jia, X. Su, Q. Pan, J. Gao, C. Xie, K. Peng, Experimental demonstration of unconditional entanglement swapping for continuous variables. *Phys. Rev. Lett.* **93**, 250503 (2004).
26. N. Takei, H. Yonezawa, T. Aoki, A. Furusawa, High-fidelity teleportation beyond the no-cloning limit and entanglement swapping for continuous variables. *Phys. Rev. Lett.* **94**, 220502 (2005).
27. S. Takeda, M. Fuwa, P. van Loock, A. Furusawa, Entanglement swapping between discrete and continuous variables. *Phys. Rev. Lett.* **114**, 100501 (2015).
28. S.-W. Lee, J. Jeong, Near-deterministic quantum teleportation and resource-efficient quantum computation using linear optics and hybrid qubits. *Phys. Rev. Lett.* **87**, 022326 (2012).
29. Y.-B. Sheng, L. Zhou, G.-L. Long, Hybrid entanglement purification for quantum repeaters. *Phys. Rev. A* **88**, 022302 (2013).
30. S. Bose, V. Vedral, P. L. Knight, Purification via entanglement swapping and conserved entanglement. *Phys. Rev. A* **60**, 194–197 (1999).
31. H. Le Jeannic, V. B. Verma, A. Cavaillès, F. Marsili, M. D. Shaw, K. Huang, O. Morin, S. W. Nam, J. Laurat, High-efficiency WSi superconducting nanowire single-photon detectors for quantum state engineering in the near infrared. *Opt. Lett.* **41**, 5341–5344 (2016).
32. A. I. Lvovksy, M. G. Raymer, Continuous-variable optical quantum state tomography. *Rev. Mod. Phys.* **81**, 299–332 (2009).
33. G. Vidal, R. F. Werner, A computable measure of entanglement. *Phys. Rev. A* **65**, 032314 (2002).
34. J.-i. Yoshikawa, K. Makino, S. Kurata, P. van Loock, A. Furusawa, Creation, storage, and on-demand release of optical quantum states with a negative wigner function. *Phys. Rev. X* **3**, 041028 (2013).
35. M. Bouillard, G. Boucher, J. Ferrer Ortas, B. Pointard, R. Tualle-Brouri, Quantum storage of single-photon and two-photon fock states with an all-optical quantum memory. *Phys. Rev. Lett.* **122**, 210501 (2019).
36. J. C. Loredo, C. Antón, B. Reznychenko, P. Hilaire, A. Harouri, C. Millet, H. Ollivier, N. Somaschi, L. De Santis, A. Lemaître, I. Sagnes, L. Lanco, A. Auffèves, O. Krebs, P. Senellart, Generation of non-classical light in a photon-number superposition. *Nat. Photonics* **13**, 803–808 (2019).
37. B. Hacker, S. Welte, S. Daiss, A. Shaukat, S. Ritter, L. Li, G. Rempe, Deterministic creation of entangled atom-light Schrödinger-cat states. *Nat. Photonics* **13**, 110–115 (2019).
38. M. Mehmet, S. Ast, T. Eberle, S. Steinlechner, H. Vahlbruch, R. Schnabel, Squeezed light at 1550 nm with a quantum noise reduction of 12.3 dB. *Opt. Express* **19**, 25763–25772 (2011).
39. O. Morin, C. Fabre, J. Laurat, Experimentally accessing the optimal temporal mode of traveling quantum light states. *Phys. Rev. Lett.* **111**, 213602 (2013).
40. S. Takeda, K. Takase, A. Furusawa, On-demand photonic entanglement synthesizer. *Sci. Adv.* **5**, eaaw4530 (2019).
41. H. Takahashi, J. S. Neergaard-Nielsen, M. Takeuchi, M. Takeoka, K. Hayasaka, A. Furusawa, M. Sasaki, Entanglement distillation from Gaussian input states. *Nat. Photonics* **4**, 178–181 (2010).
42. Y. Lim, J. Joo, T. P. Spiller, H. Jeong, Loss-resilient photonic entanglement swapping using optical hybrid states. *Phys. Rev. A* **94**, 062337 (2016).

Acknowledgments: We thank O. Morin and K. Huang for contributions in the early stages of the experiment. **Funding:** This work was supported by the European Research Council (Starting Grant HybridNet), the PERSU program from Sorbonne Université (ANR-11-IDEX-004-02), and the French National Research Agency (HyLight project ANR-17-CE30-0006). V.B.V. and S.W.N. acknowledge funding for detector development from the Defense Advanced Research Projects Agency (DARPA) Information in a Photon and QUINESS programs. G.G. was supported by the European Union (Marie Curie Fellowship HELIOS IF-749213) and T.D. by the Region Ile-de-France in the framework of DIM SIRTEQ. **Author contributions:** G.G., T.D., and A.C. performed the experiment, developed implementation techniques, and realized the data analysis. H.L.J. contributed to the preparation of the setup. V.B.V. and S.W.N. developed the single-photon detectors. J.L. designed research and supervised the project. All authors discussed the results and contributed to the writing of the manuscript. **Competing interests:** The authors declare that they have no competing interests. **Data and materials availability:** All data needed to evaluate the conclusions in the paper are present in the paper and/or the Supplementary Materials. Additional data related to this paper may be requested from the authors.

Submitted 4 December 2019
Accepted 25 March 2020
Published 29 May 2020
10.1126/sciadv.aba4508

Citation: G. Guccione, T. Darras, H. Le Jeannic, V. B. Verma, S. W. Nam, A. Cavaillès, J. Laurat, Connecting heterogeneous quantum networks by hybrid entanglement swapping. *Sci. Adv.* **6**, eaba4508 (2020).

Science Advances

Connecting heterogeneous quantum networks by hybrid entanglement swapping

Giovanni Guccione, Tom Darras, Hanna Le Jeannic, Varun B. Verma, Sae Woo Nam, Adrien Cavaillès and Julien Laurat

Sci Adv **6** (22), eaba4508.
DOI: 10.1126/sciadv.aba4508

Science Advances (ISSN 2375-2548) is published by the American Association for the Advancement of Science, 1200 New York Avenue NW, Washington, DC 20005. The title *Science Advances* is a registered trademark of AAAS.